Paper No.
13302

NACE INTERNATIONAL
CORROSION Conference & Expo 2019

Corrosion of armor wire steel in the annulus of flexible pipes at near neutral pH

Tatiane Campos
LabCorr/COPPE/UFRJ
CT, Ilha do Fundão
Rio de Janeiro/RJ, 21941-972
Brazil

Marion Seiersten
Institute for Energy Technology
P.O. Box 40,
NO-2027 Kjeller
Norway

José Antônio Gomes
LabCorr/COPPE/UFRJ
CT, Ilha do Fundão
Rio de Janeiro/RJ, 21941-972
Brazil

Simona Palencsár
Institute for Energy Technology
P.O. Box 40,
NO-2027 Kjeller
Norway

Arne Dugstad
Institute for Energy Technology
P.O. Box 40,
NO-2027 Kjeller
Norway

ABSTRACT

Stress corrosion cracking (SCC) of carbon steel may occur at near neutral pH in deoxygenated solutions with high bicarbonate concentration. Similar conditions are encountered in the annular space of flexible pipes when it is filled with CO_2 containing condensed water or seawater. The CO_2 diffuses from the bore into the annulus through the polymer sheets. Corrosion of the armor wires in contact with the water will result in high levels of Fe^{2+} and bicarbonate (HCO_3^-). Several studies have indicated that SCC may occur in solutions with high HCO_3^- concentration by production of elemental hydrogen during the corrosion reaction. The objective of the present study was to investigate if such conditions can persist for sufficiently long time in the annulus of flexible pipes to induce SCC of armor wire steel. It implies that the nucleation and growth of siderite ($FeCO_3$) is so slow that the solution remains supersaturated for days to weeks. The results show that it is possible. At temperature lower than 40 °C and CO_2 partial pressure of 10-5 kPa the saturation ratios (SR) of siderite can remain much higher than 1 and maintain a near-neutral pH for several hundred hours. However, the corrosion rate of armor wire steel at these conditions is low. Siderite precipitates at the steel surface and the cathodic reaction rate becomes diffusion controlled.

Key words: corrosion, flexible pipe, annulus, siderite, CO_2, near neutral pH, SCC.

INTRODUCTION

The annular space of flexible pipes is dry and non-corrosive at normal operating conditions. However, when flooded, with condensed water, resulting from the permeation of the production gases through the inner sheath, or seawater, due to damage to the outer sheath, the steel wires in the annulus can be exposed to corrosive conditions. The wires are high strength carbon steel, and the corrosion products are iron(II), bicarbonate and carbonate ions. It is anticipated that the water in the annular space will be saturated with iron carbonate (siderite) in relatively short time due to the low ratio between the free volume (V) and the surface area of the wires (S). [1,2] The solubility of siderite is governed by the ferrous and carbonate ions activity as defined by the solubility product for siderite K_{sp} ($mol^2.L^{-2}$) which decreases with temperature. [3-6]

$$FeCO_3(s) \rightleftarrows Fe^{2+} + CO_3^{2-} \quad (1)$$

$$K_{sp} = a_{Fe^{2+}} \times a_{CO_3^{2-}} \quad (2)$$

where a_i is the activity of the subscripted species *i*. The carbonate ion activity depends on the CO_2 partial pressure, the alkalinity, the Henry's law constant for CO_2 dissolution, as well as the formation and dissociation constants of carbonic acid; i.e. the equilibrium constants for Eq. 3 and Eq. 4. The carbonate ion concentration will increase with the pH.[7]

$$CO_3^{2-} + H^+ \rightleftarrows HCO_3^- \quad (3)$$

$$HCO_3^- + H^+ \rightleftarrows H_2CO_3 \rightleftarrows CO_2(aq) + H_2O \quad (4)$$

Most studies on CO_2 corrosion are conducted at pH lower than 6.5 as that is most relevant for oil and gas production. However, in the annulus of flexible pipes the pH can be near neutral because of the low partial pressure of CO_2 and the accumulation of corrosion products. CO_2 that diffuses through the polymer sheets, maintains a low, but noticeable concentration of dissolved CO_2 and carbonic acid in the water in the annulus. Corrosion of steel increases the alkalinity by the formation of bicarbonate ion, according to Eq. 5.

$$Fe + 2H_2CO_3 \rightarrow Fe^{2+} + 2HCO_3^- + H_2\ (g) \quad (5)$$

The alkalinity in the solution is defined as the stoichiometric sum of all titrable bases in solution minus H^+ concentration. According to Eq. 5, when the corrosion reaction is the only source of Fe^{2+} and alkalinity, and $FeCO_3$ is the only precipitate, the alkalinity will be two times the molal Fe^{2+} concentration.

If the produced gas is sweet and there is no ingress of seawater, the rates of CO_2 diffusion, corrosion, and $FeCO_3$ precipitation control the pH in a wet annulus. At low temperatures (<30 °C) the kinetics of siderite precipitation is so slow that it may maintain high Fe^{2+} concentration and a sufficient CO_3^{2-} concentration to give a saturation ratio (SR) of siderite higher than 1 (Eq. 6).[1,8]

$$SR = \frac{a_{Fe^{2+}} \times a_{CO_3^{2-}}}{K_{sp}} \quad (6)$$

where a_i is the activity of the subscripted species i and K_{sp} is the solubility product of siderite.

At high pH, the nucleation and growth of siderite govern the corrosion rate of carbon steel in CO_2 environments. When siderite forms a dense, continuous layer on the steel surface, it acts as a diffusion barrier for the species involved in the corrosion process.[9-12]

The chemical composition and microstructure of the steels affect the formation and properties of the corrosion product films covering the steel surface. The adhesion of films is related to the presence, size and distribution of carbides in the steels, which are considered important "anchors" of the corrosion products.[13-20] The steels used in armor wires have a considerably higher carbon content compared to pipeline steels and if carbides play a key role in the corrosion mechanism, high carbon steels may exhibit a different corrosion rate. It should also be noted that the armor wires develop adherent surface layers in the manufacturing process and these may also affect the corrosion mechanism.

Stress corrosion cracking has been found in near-neutral environments associated with dilute bicarbonate solutions. This problem was widely reported by National Energy Board in Canada.[21] SCC occurred in external walls of pipelines in contact with soil where the cathodic protection system did not work. Fractured surfaces were characterized as a quasi-cleavage showing transgranular cracking filled with corrosion products in the beginning, being followed by intergranular propagation of secondary cracks.

According to Asher and co-workers, secondary cracks suggest that hydrogen plays a role in the cracking mechanism.[22-23] Hydrogen is a product of the corrosion reaction (Eq. 5), i.e. the cathodic reaction (Eq. 7).

$$2H^+ + 2e^- \rightarrow 2H_{(ads)} \quad (7)$$

The adsorbed H atoms can either combine to H_2 molecules or dissolve in the steel. Asher et al. showed that cracks developed in steel exposed at low CO_2 partial pressure in electrolytes with bicarbonate ion added to near-neutral pH. The cracks started at specific sites, i.e. inclusion or pits, and the authors attributed it to higher H dissolution rate at such defects. Their results indicated that hydrogen dissolution rate and crack density were higher at 25 °C compared to 15 °C.[22]

Parkins and Zhou studied SCC of low carbon steels in CO_2-(bi)carbonate solutions by slow strain rate tests (SSRT). The cracks presented potential range dependence. Transgranular fissures were associated with potential ranges where iron dissolves and intergranular cracking with potentials where hydrogen discharge is possible. They also observed that crack growth increased with increasing bicarbonate ion concentration, suggesting that HCO_3^- is involved in the crack mechanism.[24]

The objective of this study was not to study SCC, but to investigate if conditions that lead to near neutral pH and hydrogen absorption in steel can occur in the annulus of flexible pipes. It implies to answer the following:
1) Can CO_2 corrosion of steel armor wires in the annular space of flexible pipes create a solution with high bicarbonate concentration that remains supersaturated with iron carbonate for a substantial length of time?
2) Can a protective iron carbonate layer form on typical armor wire steels?

The studies included steel specimens with machined clean surfaces and as received material which was only degreased.

EXPERIMENTAL PROCEDURE

Materials and test solutions

The materials used as corrosion coupons were tensile wires from flexible pipes. Table 1 presents their chemical compositions. Both steel #6 and #8 have a ferrite-perlite microstructure.

The siderite supersaturation evaluations were performed in distilled water. For the corrosion tests distilled water with 0.1 %wt NaCl and artificial seawater based on ASTM D1141-98 were used. In all cases, the liquids were purged with CO_2 before and during the experiments to avoid the oxidation of ferrous ions.[25]

Table 1
Chemical compositions of the tested materials.

Sample REF	C	Si	Mn	P	S	Cr	Ni	Mo	Al	Cu
#6	0.68	0.25	0.78	0.015	0.011	0.021	‹0.015	0.003	-	0.033
#8	0.66	0.24	0.76	0.018	0.018	0.043	0.02	0.005	0.034	0.012

Test system

The siderite supersaturation experiments were performed in a 1 L jacketed glass cell. The solution was gently stirred and continuously purged with a mixture of N_2 and CO_2, as indicated in Table 2, at a pressure of 100 kPa and a gas flowrate of 200 mL/min. The temperature was measured in the solution in the cell and controlled using an external thermostatic bath (Figure 1).

Alkaline ferrous solution was made in a 3 L feeding unit. It was loaded with steel wool continuously and purged with CO_2 (100 kPa). By keeping the solution at 5-12 °C, it was possible to maintain a high ferrous ion concentration in the feeding unit. An aliquot of the feed solution was transferred to the test cell and diluted with deoxygenated distilled water to achieve a solution with ca. 20 mmol/kg Fe^{2+} (1100 mg/kg). The test conditions are given in Table 2. The pH was monitored throughout the tests. The solution was sampled every 1-3 days, and filtered through 0.1 µm filters before the dissolved Fe^{2+} complexed as iron phenanthroline was measured by UV-visible spectroscopy. The alkalinity produced in the feeding unit was anticipated to be two times higher than the Fe^{2+} concentration on molal basis. The total pressure and the CO_2 concentration in the gas were used as input to the MultiScale* 8.1 software to calculate the CO_2 fugacity and the activities required to determine the saturation ratio for $FeCO_3$.

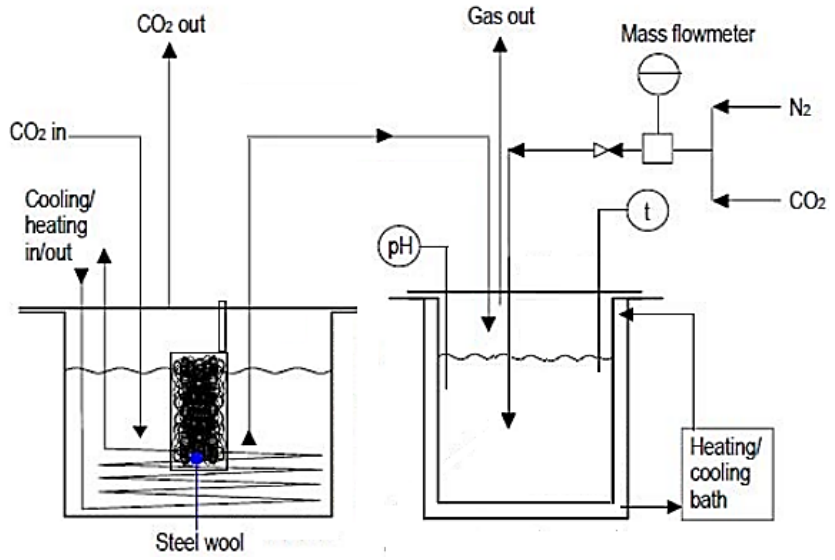

Figure 1: Schematic diagram of the test system showing the ferrous feeding unit (on the left) and the test cell (on the right).

At the end of the experiments, most of the solids were sedimented in the cell before most of the liquid was removed. The solids in the cell were dried under the gas mixture used during the tests. The dry solids were collected and analyzed by scanning electron microscopy (SEM), energy dispersive

* Trade name

spectrometry (EDS) and X-ray diffraction (XRD). The XRD spectra were measured with a scan range from 10-90 θ with a step size of 0.2 θ and a holding time of 12 s.

Table 2
Experimental test matrix (total pressure 100 kPa) (Prec.= Precipitation).

Experiment	Initial conc. (mmol/kg)		CO_2 in gas (%)	T (°C)	Salt content	Prec. tests	Corrosion tests	Steels tested
	$[Fe^{2+}]$	Alkalinity						
10C	18.50	37.00	10 to 5	10	0	x		
15C	18.20	36.40	10 to 5	15	0	x		
25C	18.54	37.08	10	25	0	x		
25C_corr	20.05	40.10	10	25	0.1% NaCl	x	x	#6 and #8 machined and as received
25C_SW_corr	18.00	36.00	10	25	Artificial seawater	x	x	#6 and #8 as received
40C	21.45	42.90	10 to 5	40	0	x		

Electrochemical measurements

A 3L jacketed cell was used for the corrosion experiments. The solutions were prepared from distilled water and >99% purity salts and deoxygenated with CO_2 purging before introducing the corrosion coupons. Ferrous ions and alkalinity were prepared in the feeding unit and transferred to test cell. The electrochemical measurements were performed in a 3-electrode set-up; the tensile wires coupons as working electrodes (WE), a titanium wire as counter electrode (CE) and an Ag/AgCl (3 M KCl) as reference electrode (RE). A Gamry potentiostat with multiplexer was used for linear polarization resistance (LPR), potentiodynamic sweeps and electrochemical impedance spectroscopy (EIS) measurements.

The corrosion rate was determined by LPR and weight loss. The LPR scans were conducted every 30 min at 0.1 mV/s, from -5 to +5 mV relative to the open circuit potential (OCP). The corrosion current density was calculated according to the Stern-Geary equation (Eq. 8):

$$i = \frac{B}{R_p A} \quad (8)$$

where A is the specimen area; Rp is the polarization resistance (Eq. 9), that is the ratio between the potential variation (E) and current (I); and B is the Stern-Geary constant calibrated against the material weight loss during the experiment. When the material loss could not be used, i.e. for the as received material, the B value was set to 20 mV (the average obtained for the machined specimen).

$$R_p = \frac{\Delta E}{\Delta I} \quad (9)$$

The corrosion rate is a function of the corrosion current density (i_{corr}), molar mass of iron, steel density and a constant defined by the units. It can be expressed according to Eq.10.

$$CR\ (mm/y) = 1.16\left(\frac{m^2 mm}{Ay}\right) i_{corr}(A/m^2) \quad (10)$$

Cathodic polarization sweeps were done several times throughout the experiments by varying the potential from +5 to -300 mV relative to the open circuit potential (OCP), at 0.1 mV/s sweep rate. Anodic polarization sweeps from -5 to +50 mV vs. OCP were done at the end of each experiment.

All polarization resistance measurements were corrected for the solution resistance (R_s) as determined by EIS. The EIS measurements were performed immediately before the cathodic sweeps. The frequency range was 0.05 to 10000 Hz, the AC voltage was 10 mV vs. E_{corr}, and 6 points were recorded per decade.

RESULTS

Siderite precipitation rate

Five experiments were performed at varying temperature and salinity. Table 2 shows the test matrix. The experiments started by adding ferrous ion rich solution to give a concentration of 1100 ppm Fe^{2+} which corresponds to 20 mmol/kg Fe^{2+} and 40 mmol/kg of alkalinity. The alkalinity was mainly bicarbonate (see Eq. 5). The CO_2 partial pressure was ca. 10 and 5 kPa respectively (the purge gas was 10 and 5 mol% respectively CO_2 in N_2 and became saturated with water) in the precipitation experiments and 10 kPa in the combined corrosion and precipitation experiments.

Figure 2 shows the influence of temperature, salinity and CO_2 partial pressure on the pH, Fe^{2+} concentration and $SR_{(siderite)}$. The rate of the pH change decreased with time and the calculated equilibrium pH (precipitation to SR=1) as given in Table 3 was not reached at any temperature. The pH increased when the CO_2 partial pressure was reduced from 10 to 5 kPa and for a short time after the pressure reduction, the pH change rate with time increased slightly.

Table 3
Expected pH at equilibrium (SW = artificial seawater solution).

Temperature		10 °C	15 °C	25 °C	25 °C_SW	40 °C
pH at equilibrium	**10% CO_2**	6.07	6.05	6.01	6.17	5.98
	5% CO_2	6.27	6.25	6.21	6.37	6.18

The Fe^{2+} concentration decreases with time as shown in Figure 2b. At low temperature, the Fe^{2+} concentration is nearly constant for a period before it starts to decrease. At 40 °C the Fe^{2+} concentration decreases to 120 ppm in less than 20 hours. At 10 and 15 °C there is a small, but evident decrease in Fe^{2+} concentration when the CO_2 partial pressure is reduced (at ~350 and ~220 hours, respectively).

The $SR_{(siderite)}$ as function of time is shown in Figure 2c. At low temperature, it remained at values much higher than 1 for several hundred hours. At 40 °C, it decreased to less than 10 in 100 hours. At all temperatures, the $SR_{(siderite)}$ increases when the pressure is reduced. The pressure reduction induced a slightly faster precipitation before the SR became nearly constant with time. At 40 °C, the Fe^{2+} concentration apparently did not change after the CO_2 partial pressure reduction and there is no decrease in the SR either. This might indicate that not all solids could be removed by filtering and would result in a higher estimated alkalinity and pH. This was observed in some of the experiments and is discussed later.

Two of the experiments performed at 25 °C were in the presence of corrosion coupons and additional salts. The coupons and solid $CaCO_3$ (expected to form in artificial seawater) might introduce surfaces which enhance the nucleation and growth. However, the de-supersaturation rate is not faster in the experiments with corrosion coupons.

The presence of Ca^{2+} in artificial seawater may have an effect if $CaCO_3$ precipitates. The consequence will be a faster pH decrease and lower Fe^{2+} consumption as observed, see Figure 2a and Figure 2b. As

discussed below, none of the $CaCO_3$ polymorphs were identified in the collected solids, but the effect will be the same if Ca^{2+} substitutes Fe^{2+} in siderite. When it is assumed that the $CaCO_3$ precipitates to equilibrium early in the experiment, the SR for $FeCO_3$ will follow the curve shown in Figure 2c. However, it should be noted that the higher ionic strength of the seawater has a significant effect on the activity coefficient of Fe^{2+} and hence the SR.

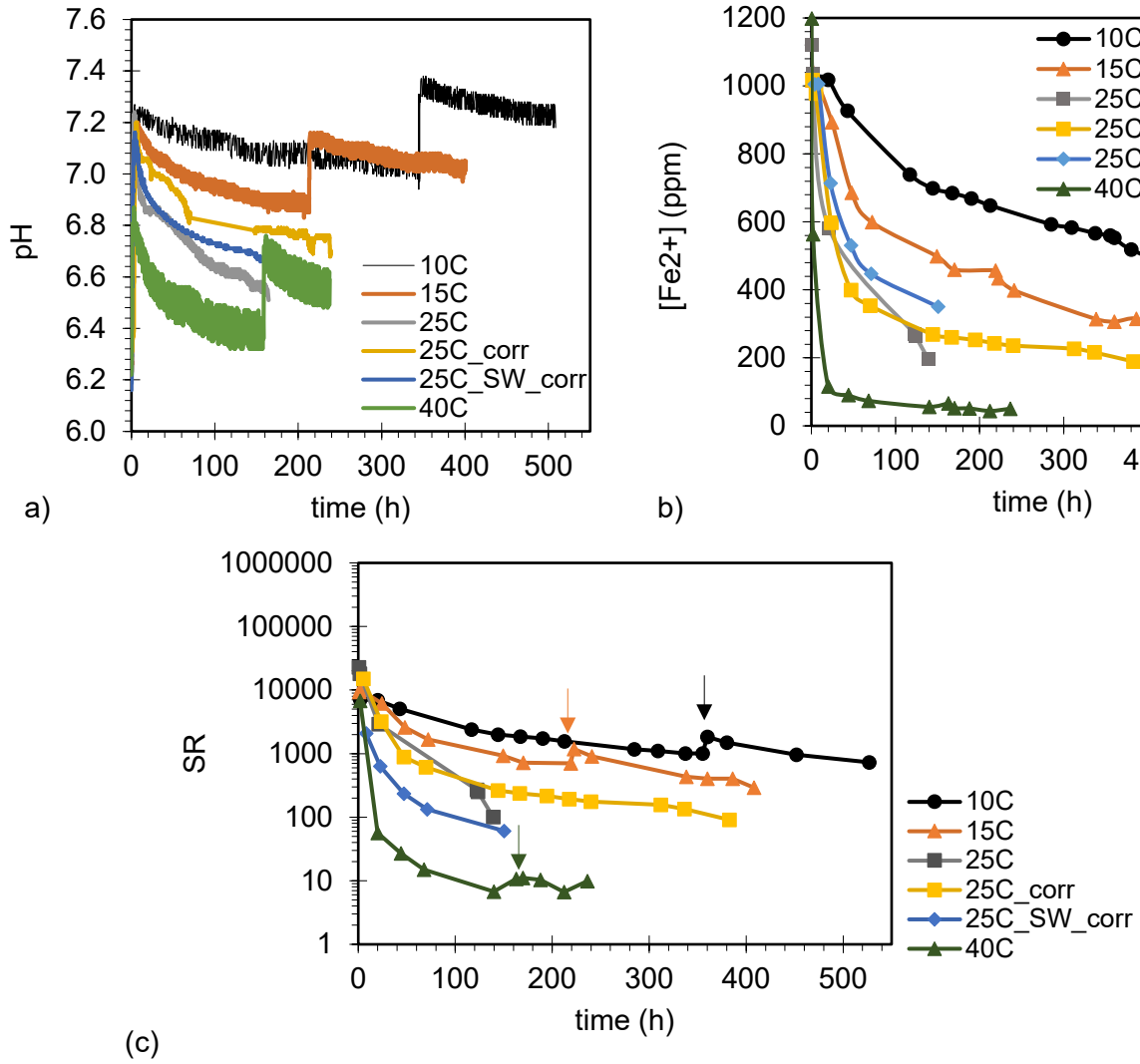

Figure 2 – Supersaturation experiments (a) measured pH; (b) measured [Fe^{2+}]; (c) resulting $FeCO_3$ SR vs. time. The arrows in (c) show when the CO_2 partial pressure was decreased from 10 to 5 kPa (SW = artificial seawater solution, corr = tests with corrosion coupons).

XRD and EDS analyses of the solid products collected at the end of exposure confirmed the presence of siderite at all test conditions. Chuckanovite ($Fe_2(OH)_2CO_{3(s)}$) was also detected by XRD at 25 °C (0.1% NaCl) and 40 °C (Figure 3). It is metastable and probably an intermediate species which transforms to siderite as exemplified by Eq. 11 and 12.[26]

$$2Fe^{2+} + HCO_3^- + 3OH^- = Fe_2(OH)_2CO_{3(s)} + H_2O \quad (11)$$

$$Fe(OH)_2CO_3(s) + CO_3^{2-} \rightarrow 2FeCO_3(s) + 2OH^- \quad (12)$$

NaCl was also detected in artificial seawater experiments as seen in the XRD spectrum. It precipitates when the water dries up. A shift in peak position for siderite in the sample collected from the seawater experiment, compared to the others, may be attributed to the presence of calcium in the crystal structure.

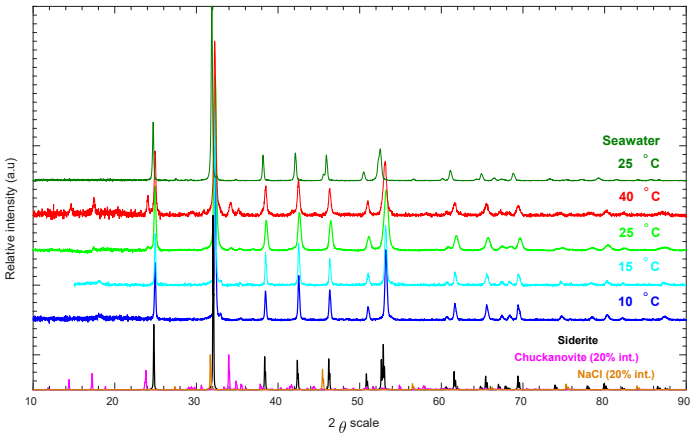

Figure 3 – XRD results for the products formed at different temperatures.

Corrosion of armor steel in highly supersaturated solutions at near neutral pH at 25 °C

Corrosion experiments were run at room temperature and 10 kPa CO_2. The solutions were supersaturated with corrosion products from the start. The pH stabilized at near-neutral levels as shown in Figure 4. The curves show the pH as function of the Fe^{2+} concentration. The pH calculated is the value estimated by assuming that the alkalinity is twice the Fe^{2+} concentration (molal). It is higher than the measured pH, especially at higher Fe^{2+} concentration; i.e. in the beginning of the experiments. It might indicate that small siderite particles not captured in the filter during sampling lead to an overestimate of the alkalinity. It also results in reported SR values that are higher than the actual values in the solution. However, towards the end of the experiments the estimated and measured pH are close, and then the error in the SR values will be minor. In the artificial seawater, the measured and calculated pH values are close if it is assumed that calcite precipitates to equilibrium (Ca consumption) early in the experiment.

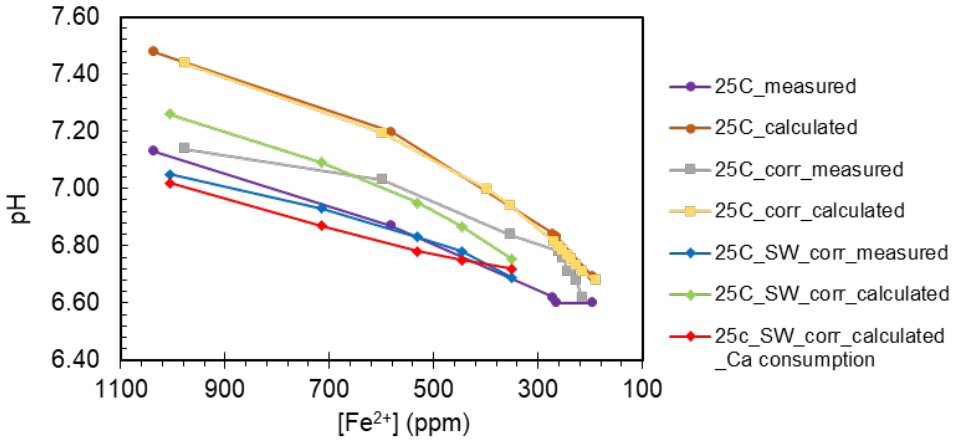

Figure 4 – Measured and calculated pH of distilled water (25C), 0.1% NaCl (25C_corr) and seawater (25C_SW_corr) solutions at room temperature as a function of ferrous ion concentration. (measured = measured values, calculated = estimated based on analyzed Fe^{2+} SW = artificial seawater solution, corr = tests with corrosion samples)

<u>0.1% NaCl solution</u>

The corrosion rates of the two steels, #6 and #8, with different surface finish (machined or as received) is shown in Figure 5. The coupons with machined surface have a slightly higher corrosion rate. This can be related to the presence of oxides and lubricants on the surface or a higher surface area of the as received materials. The initial corrosion rate is in the range 0.1 to 0.4 mm/y and it declines to 0.01 mm/y or less after a few hours. The low corrosion rate is maintained throughout the experiment. The

discontinuities in the curves are due to the cathodic sweeps and impedance measurements performed during the experiments which caused some disturbances on the surface of the samples. This can also be observed in Figure 9.

The cathodic reactions are under diffusion control, an indication that the protective layers on the surface limit the amount of bicarbonate ions and/or protons that reaches the reaction sites. The limiting current decreases somewhat with time (Figure 6). The impedance spectra (Figure 7) also indicate that a high resistivity surface film develops with time. The presence of a dense film on the surface is confirmed by pictures as shown in Figure 8. Both steel types were completely covered with siderite. The cross sections revealed some gaps in the film. However, no evidences of localized corrosion were found on stripped samples.

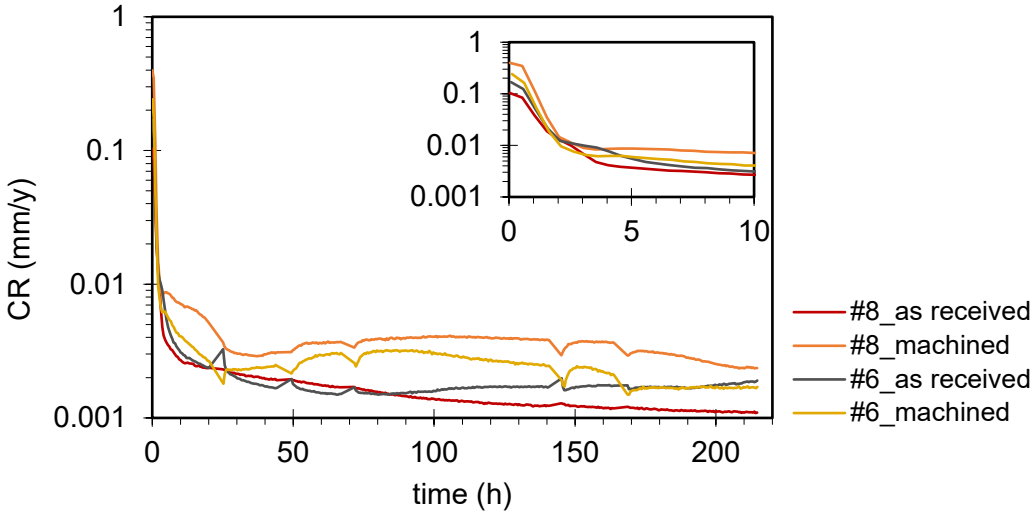

Figure 5 – Corrosion rate at 25 °C in 0.1% NaCl solution with high Fe^{2+} concentration and alkalinity. Two different steels (Table 1) with machined and as received surface finish.

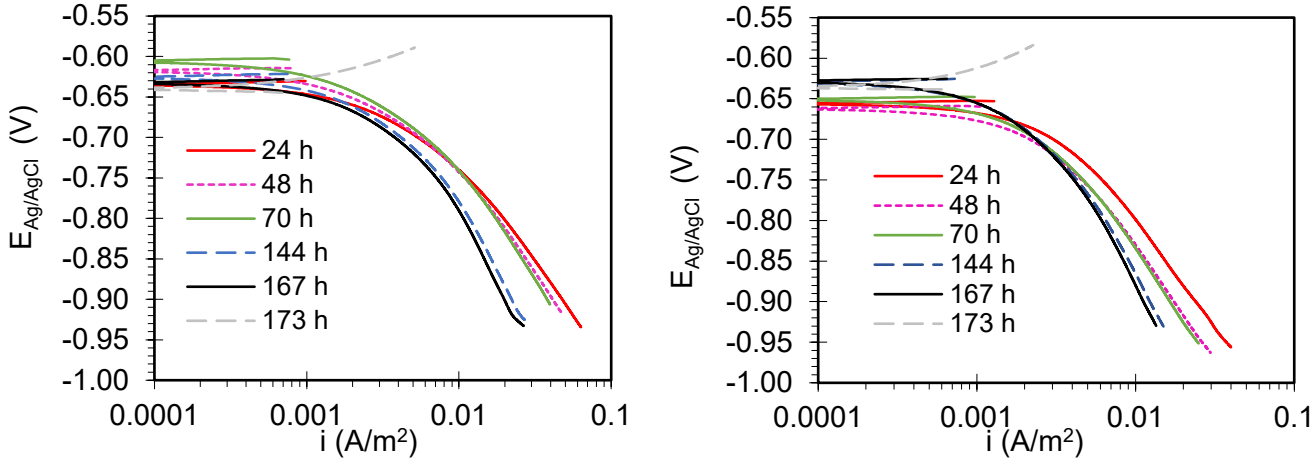

Figure 6 – Potentiodynamic sweeps for (left) #6 as received and (right) #8 as received at 25 °C in 0.1% NaCl solution.

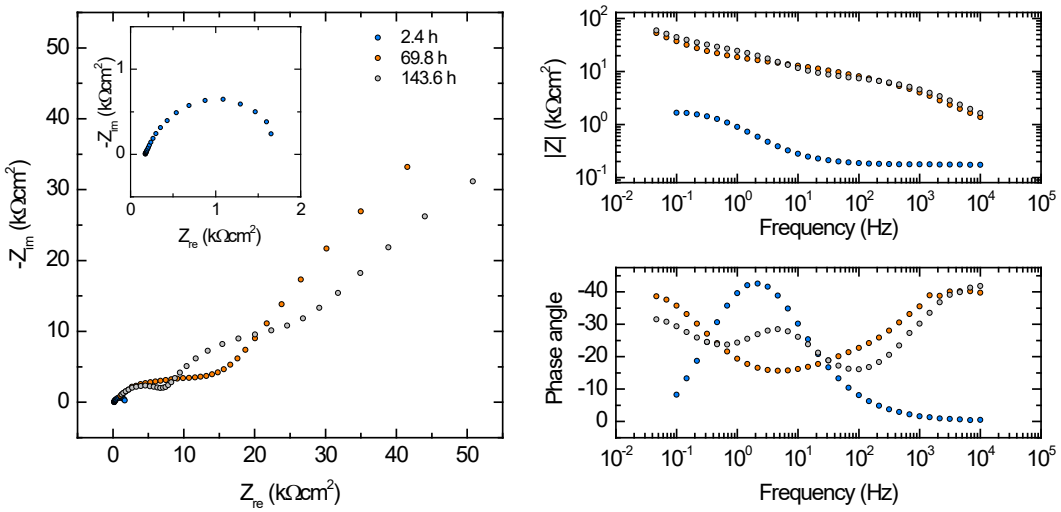

(a)

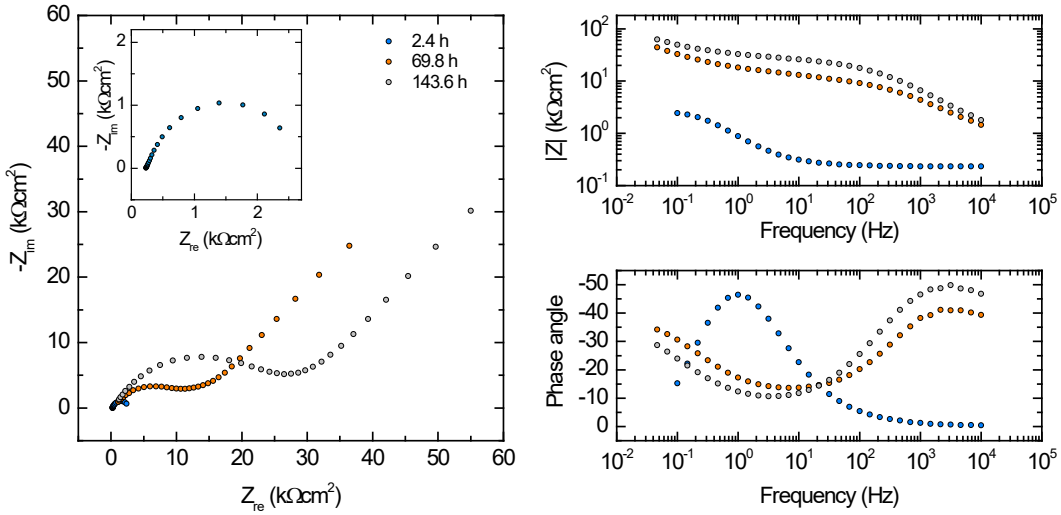

(b)

Figure 7 - EIS for (a) #6 as received and (b) #8 as received at 25 °C in 0.1% NaCl solution.

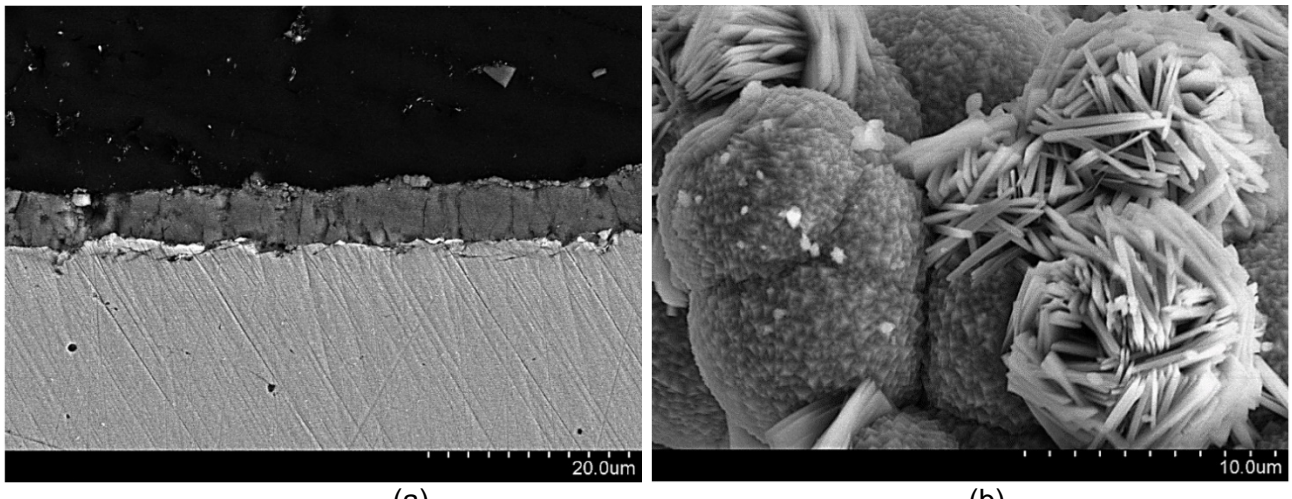

(a) (b)

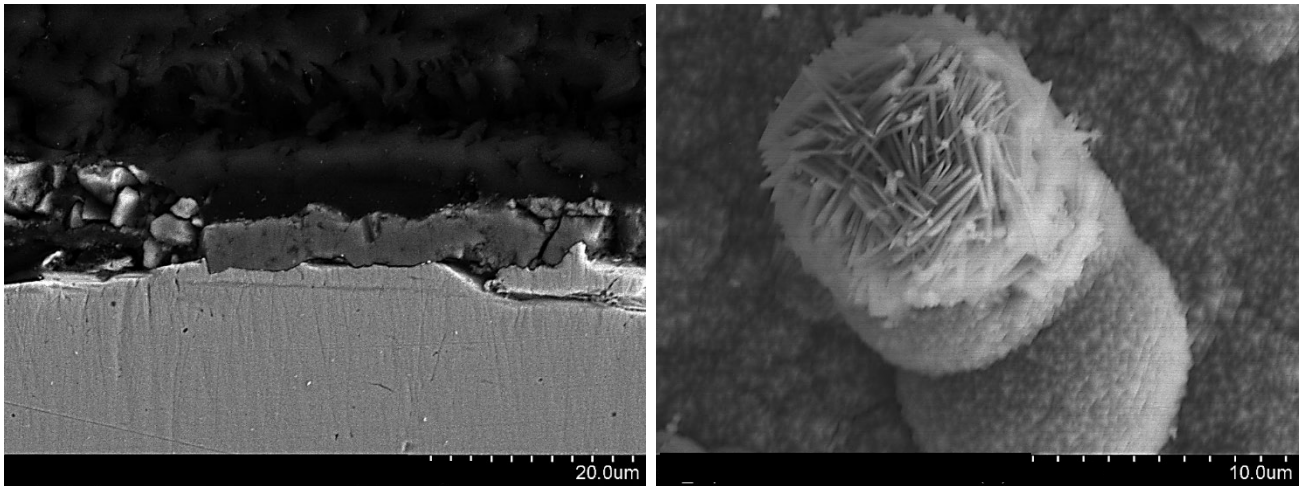

(c) (d)

Figure 8 – SEM images of corrosion films formed in 0.1% NaCl solution with high Fe^{2+} concentration and alkalinity. (a) and (c) cross sections of #6 and #8 steel, respectively; (b) and (d) the surface of #6 and #8 steel, respectively.

Artificial seawater

The initial corrosion rate is in the range of 0.4 to 0.1 mm/y and it declines to less than 0.01 mm/y after a few hours. The low corrosion rate is maintained throughout the experiment (Figure 9).

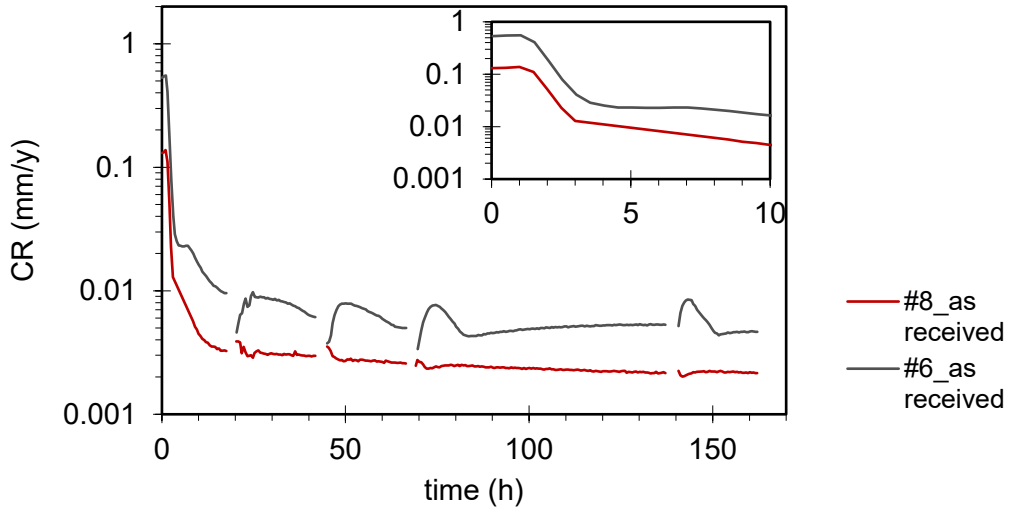

Figure 9 – Corrosion rate of armor steel at 25 °C in artificial seawater solution with high Fe^{2+} concentration and alkalinity.

The cathodic sweeps, shown in Figure 10, were similar to the ones recorded in 0.1% NaCl, indicating diffusion-controlled reactions due to the protective layers on the surface. However, there were some additional features on steel #6 at about -0.3 V vs. OCP, which indicates the reduction of a species close to the surface. Again, the cathodic limiting current decreased over time, indicating that the film became more protective with time. The impedance spectra (Figure 11) also indicate that a surface film develops with time.

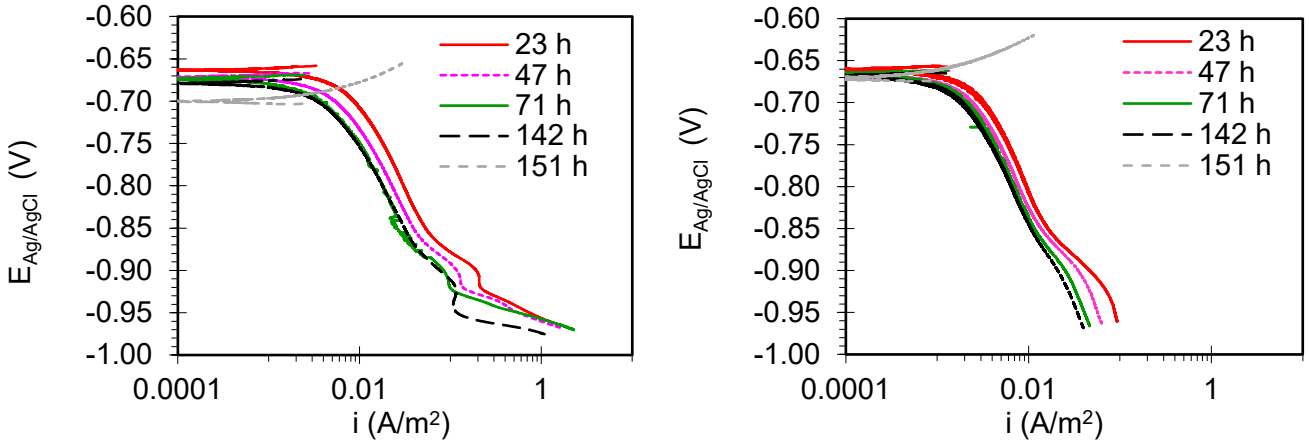

Figure 10 – Potentiodynamic sweeps from (left) #6 and (right) #8 at 25 °C in artificial seawater solution.

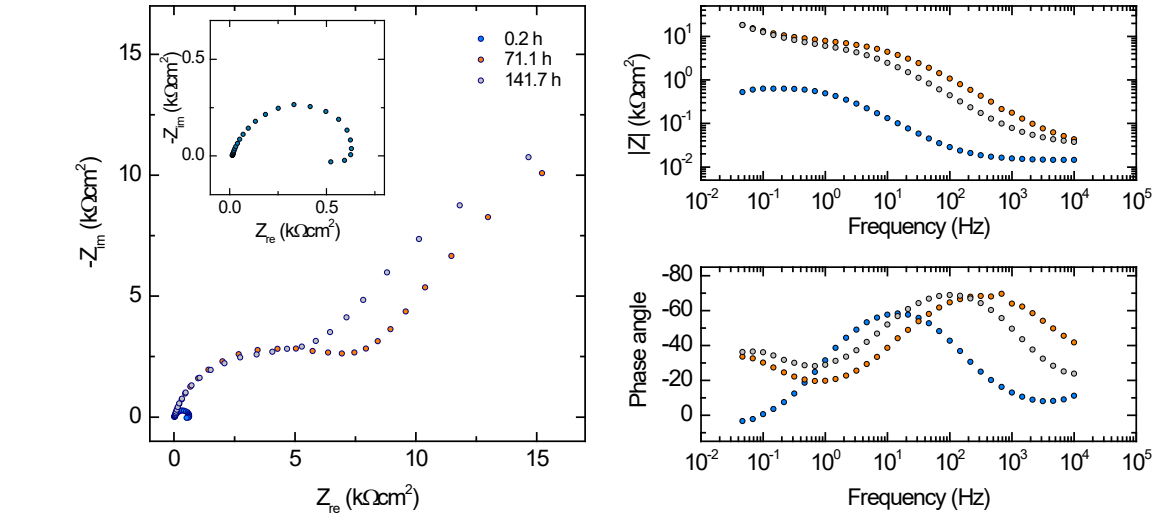

a)

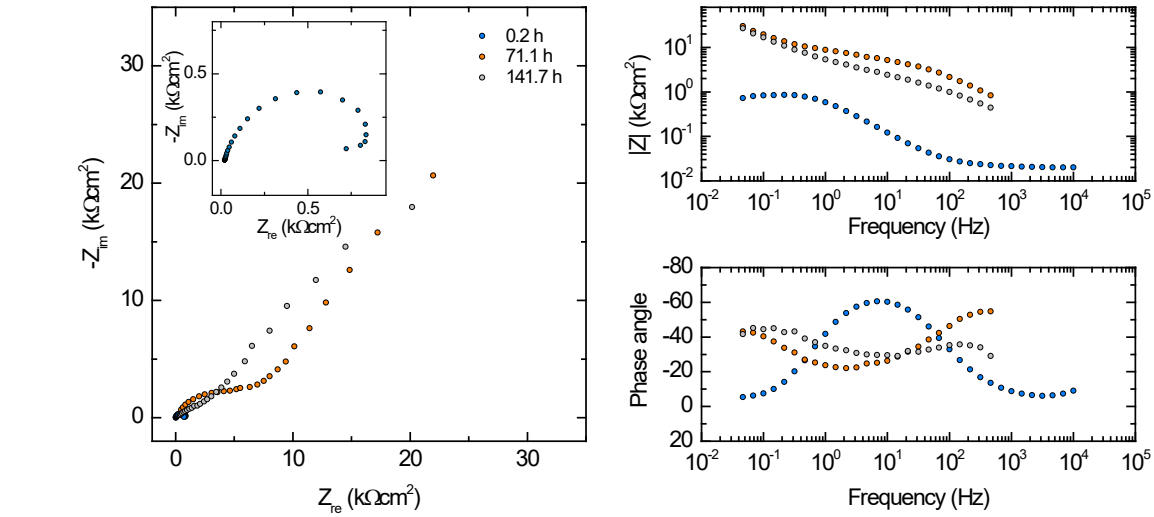

b)

Figure 11 - EIS for (a) #6 as received and (b) #8 as received at 25 °C in artificial seawater.

Figure 12 shows the SEM images of steel surfaces and cross-sections after exposure. Both steel types were completely covered with a dense layer. EDS analyses indicated siderite with some calcium. The cross section revealed some gaps in the film. However, no evidences of localized corrosion were found on stripped samples.

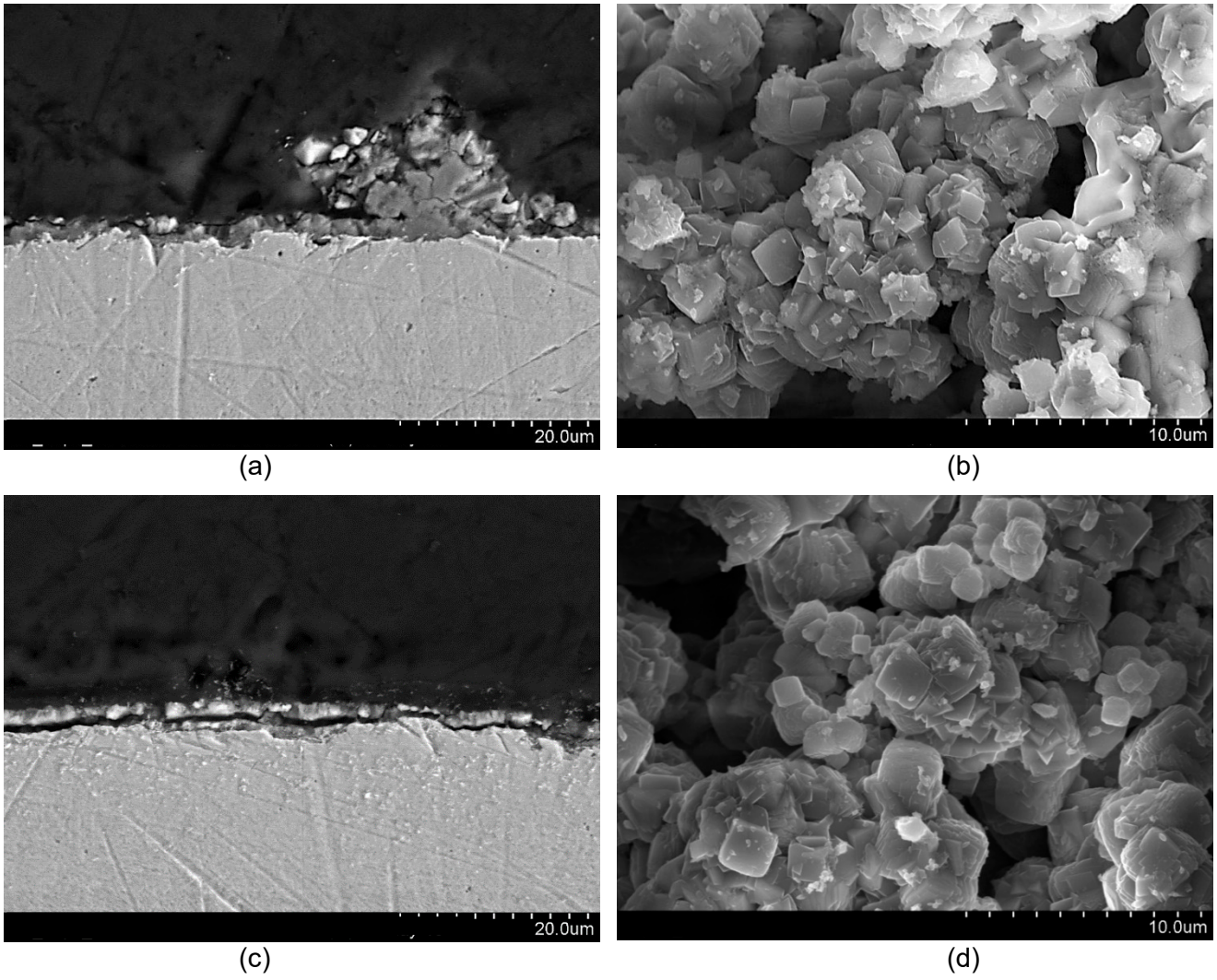

Figure 12 – SEM images of corrosion films formed in seawater solution with high Fe^{2+} concentration and alkalinity. (a) and (c) cross sections of steel #6 and #8, respectively; (b) and (d) surfaces of steel #6 and #8, respectively.

CONCLUSIONS

The saturation ratios (SR) of siderite can remain much higher than 1 and keep a near-neutral pH for long time, which can produce conditions for SCC according to literature. The SR decrease with time is faster at higher temperatures.

Protective corrosion product films formed fast at room temperature in supersaturated environments, as encountered in annular space of flexible pipes. Fully protective films giving corrosion rate less than 0.01 mm/y, formed after few hours of exposure when the SR was above 1000. The as received and machined samples exhibited somewhat different corrosion rates during the first few hours of the experiment at 0.1% NaCl solution. However, all of them remained below 0.01 mm/y after some point and

that is usually considered as low and acceptable in armor wires of flexible pipes. At this low corrosion rate, the variations in rate between coupons made from different steels and with different surface treatments is within the measuring uncertainty.

ACKNOWLEDGEMENTS

CNPq and Shell's financial support to T. Campos' PhD project and Shell's financial support to the work at IFE is greatly acknowledged. The authors also want to express gratitude to Shell and 4Subsea personnel for encouraging and valuable inputs to the work.

REFERENCES

1. A. Dugstad, S. Palencsar, L. Børvik, P.A. Eikrem, "Corrosion Testing of Steel Armour Wires in Flexible Pipes – A Parametric Study", CORROSION 2015, paper no. 5829, (Houston TX: NACE 2015).

2. E. Remita et al., "Experimental and theoretical investigation of the uniform corrosion in the annulus of offshore flexible pipelines", CORROSION 2008, paper no. 08538 (Houston TX: NACE 2008)

3. N. Désamais, C. Taravel-Condat, "On the Beneficial Influence of a Very Low Supply of H_2S on the Hydrogen Embrittlement Resistance of Carbon Steel Wires in Flexible Pipe Annulus", Offshore Technology Conference 2009, paper no. OTC-19950-MS (OTC 2009)

4. T. Epsztein et al., "New Anti H_2S Layer for Flexible Pipes", Offshore Technology Conference 2011, paper no. OTC-21371-MS (OTC 2011)

5. E. Remita et al., "A kinetic model for CO_2 corrosion of steel in confined aqueous envionment", Journal of the Electrochemical Society 155, 1 (2008) C41-C45.

6. W. Sun et al., " The effect of temperature and ionic strength on iron carbonate ($FeCO_3$) solubility limit", Corroion Science 51,6 (2009), p. 1233-1276.

7. R. D. Braum, "Solubility of iron(II) carbonate at temperatures between 10 and 80 °C", Talanta 38, 2 (1991), p. 205-211.

8. T. Berntsen, M. Seiersten, T. Hemmingsen, "Effect of FeCO3 supersaturation and carbide exposure on the CO2 corrosion rate of carbon steel", Corrosion 69, 6 (2013): p. 601-613.

9. W. Sun, S. Nesic, R.C. Woollam, "The effect of temperature and ionic strength on iron carbonate ($FeCO_3$) solubility limit", Corrosion Science 51, 6 (2009), p. 1273-1276.

10. D. Burkle, R. De Motte, W. Taleb, A, Kleppe, T. Comyn, S.M. Vargas, A. Neville, R. Barker, "In situ SR-XRD study of FeCO3 precipitation kinetics onto carbon steel in CO2-containing environments: The influence of brine pH", Electrochimica Acta 255 (2017) p. 127-144.

11. W. Sun; S. Nesic, "Kinetics of corrosion layer formation: Part 1 – Iron carbonate layers in carbon dioxide corrosion", Corrosion 64, 4 (2008), p. 334-346.

12. S. Nesic, "Key issues related to modelling of internal corrosion of oil and gas pipelines – A review. Corrosion Science 49, 12 (2007), p. 4308-4338.

13. A. Dugstad, "Mechanism of protective film formation during CO_2 corrosion of carbon steel", CORROSION 1998, paper no. 98031 (Houston TX: NACE 1998)

14. L.R.M Ferreira. et al., “A formação da camada protetora de FeCO3 e o controle da corrosão por CO2 em condiçoes de fluxo turbulento”, Quim. Nova 39, 9 (2016), p.1027–1033.

15. D. López et al., “The influence of carbon steel microstructure on corrosion layers An XPS and SEM characterization”, Applied Surface Science 207, 1-4 (2007), p.69–85.

16. J.L. Crolet, N. Thevenot, S. Nesic, “Role of Conductive Corrosion Products in the Protectiveness of Corrosion Layers”, Corrosion Science 54, 3 (1998), p.194–203.

17. A. Dugstad, H. Hemmer, M. Seiersten, “Effect of steel microstructure upon corrosion rate and protective iron carbonate film formation”, Corrosion 57, 4 (2001), p. 369-378.

18. M. Ueda, H. Takabe, “Effect of environmental factor and microstructure on morphology of corrosion products in CO_2 environments”, CORROSION 1999, paper no. 99013 (Houston TX: NACE 1999)

19. M.B. Tomson, U. Rice, M.L. Johnson, “How Ferrous Carbonate Kinetics Impacts Oilfield Corrosion”, SPE International Symposium on Oilfield Chemistry 1991, paper no SPE-21025-MS (SPE 1991),

20. Z. Liu et al., “Corrosion behavior of low-alloy steel with martensite/ferrite microstructure at vapor-saturated CO2 and CO2-saturated brine conditions”, Applied Surface Science 351 (2005), p.610–623.

21. Canada. National Energy Board Cananda. “Public inquiry concerning stress corrosion cracking on Canadian oil and gas pipelines”, (Calgary – Alberta, Canada: National Energy Board November 1996), Available at http://publications.gc.ca/site/eng/418383/publication.html

22. S. L. Asher, P. M. Singh, J. A. Colwell, B. N. Lei, “Stress corrosion cracking of pipeline steel in near-neutral pH environments”, CORROSION 2006, paper no. 06175 (Houston TX: NACE 2006).

23. J. A. Colwell, B. N. Leis, P. M. Singh, “Recent developments in characterizing the mechanism of near neutral pH SCC”, CORROSION 2005, paper no. 05161 (Houston TX: NACE 2005).

24. R.N. Parkins, S. Zhou. “The stress corrosion cracking of C-Mn steel in CO_2^{-}-HCO_3^{-}-CO_3^{2-} solutions. I: Stress corrosion data”, *Corrosion Science* 39, 1(1997), p. 159-173.

25. ASTM D1141-98. “Standard Practice for the Preparation of Substitute Ocean Water” (ASTM 2003).

26. T. Tanupabrungsun, D. Young, B. Brown, S. Nesic. “Construction and Verification of Pourbaix Diagrams for CO2 Corrosion of Mild Steel Valid up to 250 °C”. CORROSION 2012, paper no.1418 (Houston TX: NACE 2012)